RSC Advances

This article can be cited before page numbers have been issued, to do this please use: N. Gao, X. Jiang and Y. Liu, *RSC Adv.*, 2014, DOI: 10.1039/C4RA12694G.

ROYAL SOCIETY OF CHEMISTRY

www.rsc.org/advances

View Article Online
DOI: 10.1039/C4RA12694G

Graphical Abstract

Dipropargyl Ether Bisphenol A Based Boron-containing Polymer: Synthesis, Characterization and Molecular Dynamics Simulations of the Resulting Pyrolysis and Carbonization

Ning Gao, Jiang Xue, Yuhong Liu *

Department of Chemical Engineering, School of Chemical Engineering and Technology, Xi'an Jiaotong University, Xi'an 710049, China

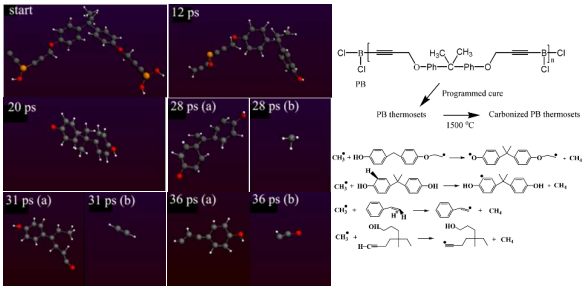

The time evolution of major pyrolysis products including small-molecule species of a dipropargyl ether bisphenol A based novel boron-containing polymer were examined via ReaxFF-MD simulation to elucidate complicated mechanisms and the dominant reaction pathways on molecular level (Snapshot of a large graphitic precursor structure formed after a simulation run time of 2.72 ns at 2300 K (Color code: C, grey; O, red; H, white; B, yellow).)

View Article Online
DOI: 10.1039/C4RA12694G

Journal Name

RSCPublishing

ARTICLE

Dipropargyl ether bisphenol A based boron-containing polymer: Synthesis, characterization and molecular dynamics simulations of the resulting pyrolysis and carbonization

Cite this: DOI: 10.1039/xoxxoooooox

Received ooth January 2012,
Accepted ooth January 2012

DOI: 10.1039/xoxxoooooox

www.rsc.org/

N. Gao,[a] X. Jiang,[a] Y. H. Liu [a,]*

Boron-containing polymers have recently attracted worldwide attention due to its ability to affect the thermal and oxidation resistance of the in situ formed material during pyrolytic carbonization. In this work, a novel dipropargyl ether bisphenol A based boron-containing polymer (PB), which can thermally cure via propargyl groups, was synthesized. PB was characterized via Fourier Transform infrared spectroscopy and nuclear magnetic resonance (^{1}H, ^{11}B and ^{13}C). Thermogravimetric analysis indicated the outstanding thermo-oxidative stability of PB thermosets with the temperature of 5% weight loss of 362 °C and char yield of 56.7% at 800 °C in air, while those are 416 °C and74.0%,respectively, in nitrogen. The time evolution of major pyrolysis products including pyroysis mechanism of PB thermosets were examined via thermogravimetry-Fourier transform infrared spectra as well as reactive molecular dynamics (ReaxFF-MD) simulations. In addition, the carbonized structure of PB thermosets was analyzed using X-ray photoelectron spectroscopy and X-ray powder diffraction. Formation of the graphitic fragment was simulated with ReaxFF-MD. Combined the ReaxFF-MD simulation with the experimental analysis, the way that boron atoms insert into the graphitic structure was illustrated.

Introduction

High temperature resistant resins are a promising class of matrices of composites able to be used as thermostructural and ablative materials. Over the last few decades, many kinds of high performance resins have been explored and they have exhibited remarkable application in aeronautics and astronautics [1-3]. For example, polyarylacetylene (PAA) resin is a highly cross-linked acetylene-terminated resin composed with only carbon and hydrogen, and thus has marvelous ablative properties [4]. However, ablative materials are susceptible to oxidation at elevated temperatures, which is a critical limitation for their widespread application in harsh environment [5-7]. Furthermore, with the rapid demand for high performance ablative materials, superior thermal-mechanical properties are of high interest. Conventional methods for protecting ablative materials from oxidation rely on using an oxidation resistant ceramic coating. This approach is only partially successful since the large mismatch between substrate and ceramic coating is likely to cause cracks, and therefore, oxidation resistance becomes invalid as the coating is cracked [8, 9]. An alternative strategy to improve the oxidation resistance and thermal stability is incorporating such hetero-atoms as B, P and Si into a polymerizable low molecular weight oligomer [10-12]. When polymeric materials containing hetero-atoms are pyrolyzed under an oxidative environment, protective inorganic oxides are formed on the surface at elevated temperatures that can protect the interior from further oxidation. Up to now, doping boron into carbon materials is an efficient route to improve thermal and oxidation resistance properties of carbon materials. Both graphitic degree and the crystallite dimension increase due to boron-catalyzed graphitization [13]. Further, a glassy boron oxide layer was formed on the surface of the carbon materials and provided an impermeable layer, precluding the passage of dry oxygen [14]. Despite the successful integration of boron into the carbon structure, the method of doping has some disadvantages. One of the major disadvantages is the necessity of employing high temperatures for doping reaction. High temperatures cost more energy and have a higher requirement for equipment, which are not feasible for large-scale industrialization. The other common disadvantage with doping is that boron is difficult to disperse uniformly in the carbon materials, and the concentration of boron in the carbon materials is in the form of a gradient which decreases as the distance from the surface of the materials increases [15]. In these cases, fabricating inorganic and organic units in a polymer chain other than doping boron into the

View Article Online
DOI: 10.1039/C4RA12694G
Journal Name

precursor resin will significantly improve the structure and surface energy.

In addition to incorporating boron atoms into polymer chain to expand industrial applicability of this new category of materials, another challenge for achieving the successful application of boron-containing polymer in ablative materials is that the relationship between the pyrolysis and the resulting structure remains largely unexplored. It was recognized that boron atoms can insert into the carbonaceous structure in situ during pyrolysis. Both reactive endothermic and pyrolysis processes involve a complex sequence of reactions, and actual exploitation of the reactions is still in its infancy. Further development of the ablative materials will require fundamental understanding of these molecular processes and the subsequent char evolution under transient conditions [16]. Through the last decades, molecular dynamics (MD) simulations have been utilized to study the dynamics of cross-linking process and structure-property relationship of cross-linked polymers and their composites [17-21]. For instance, ReaxFF molecular dynamics (ReaxFF-MD) has been successfully applied to complicated chemical reactions, such as pyrolysis of polymers [16, 22], which not only provides consistent data with experiments analysis, but also offers an alternative route to elucidate complicated mechanisms and the dominant reaction pathways on molecular level. These results can't be obtained by conventional experimental characterizations.

In the paper, we synthesized a novel dipropargyl ether bisphenol A based boron-containing (PB) precursor polymer that can thermally cure and possesses outstanding heat resistance at elevated temperature while maintaining the processability of low molecular weight compounds. First, synthesis, characterization, and thermal analysis of this novel PB polymer and the resulting PB thermosets were investigated. Subsequently, the carbonized structure of PB thermosets was characterized in depth with X-ray photoelectron spectroscopy (XPS) and X-ray powder diffraction (XRD) measurements. Specially, ReaxFF-MD simulation was performed toward elucidating the complex pyrolysis pathway of PB thermosets and the detailed chemistry of the resulting carbonized material.

Experimental

Materials

Propargyl bromide (80 wt% solution in toluene), boron trichloride (1 M solution in CH_2Cl_2), n-butyllithium (1.6 M solution in hexanes) were purchased from J&K Scientific Ltd. and used without further purification. Tetrabutyl ammonium bromide was obtained from Sinopharm Chemical Reagent Co. Ltd.. Sodium hydroxide was purchased from Hongyan Chemical Work. (Tianjin, China). Bisphenol A was chemically pure and obtained from Fuchen Chemical Work. (Tianjin, China). Toluene, hexane and tetrahydrofuran were dried according to the standard procedures prior to use. All other chemicals were analytically pure.

Synthesis of dipropargyl ether bisphenol A

A 250 mL flame-dried flask was equipped with a condenser and a magnetic stirrer. 11.400 g (50 mmol) bisphenol A, 0.200 g (0.62 mmol) tetrabutyl ammonium bromide, 6.000 g (150 mmol) of sodium hydroxide dissolved in 50 mL H_2O were added to the flask under a nitrogen atmosphere. The mixture was stirred for 3 h while keeping the temperature at 40 ^oC. Then, 14.2 mL (80 wt% solution in toluene) propargyl bromide was slowly added over a period of 20 min and the mixture was kept at 40 °C for 12 h. After removing the solution fraction by filtration, the obtained crude solid was washed using ethanol and distilled water for three times. The resulting solid powder was recrystallized with methanol to obtain about 9.570 g of dipropargyl ether bisphenol A product.

Synthesis of dipropargyl ether bisphenol A di-lithium

The subsequent reaction was performed in a 99.99% ultra-high pure nitrogen atmosphere. In a 100mL three-necked flask, equipped with a magnetic stirrer, 5.236 g (18 mmol) dipropargyl ether bisphenol A dissolved in 20 mL tetrahydrofuran was added. After cooling the solution to -78 °C using dry ice/acetone bath, 22.5 mL n-BuLi (1.6 M solution in hexane) was injected into a dropping funnel and added dropwise over 30 min to the stirred solution. A brown suspension was observed as n-BuLi was added. The mixture was continuously stirred at -78 °C for 1 h. Subsequently, the cold bath was removed and the mixture was kept at room temperature for 2 h. The brown solid powder (yield, 4.412 g) was isolated, washed with hexane and kept in a vacuum oven at 50 °C for 24 h.

Synthesis of dipropargyl ether bisphenol A boron-containing (PB) precursor

In a flame-dried 100mL three-necked flask, equipped with a magnetic stirrer and flushed with N_2, 1.500 g (4.7 mmol) of dipropargyl ether bisphenol A di-lithium was suspended in 15 mL toluene. 5.2 mL boron trichloride which was cooled to -30 °C before syringed into a dropping funnel. The dropping funnel was kept cold by equipped with a spiral copper pipe which was full of -30 °C ethanol. Then, BCl_3 was added dropwise to the flask. The reaction was kept at 0 °C during the course of addition, then it was allowed to slowly warm to room temperature. After stirring for additional 2 h, the toluene, CH_2Cl_2 and residual boron trichloride were evaporated off on a vacuum line. The product from the reaction was dissolved in THF. The soluble fraction was isolated by filtration. PB, a pale yellow powder (yield, 0.910 g) was obtained by evaporating THF on a vacuum line. PB was stored in a dryer until use.

Cross-linking of PB precursor and pyrolysis of the PB thermosets

To remove any volatile material, PB was heated at 80 °C in a vacuum oven before cure. The curing procedure of PB is defined by DSC measurement. PB samples were placed into a tube furnace and heated (10 °C/min) in a sequence at 200 °C (1 h), 220 °C (1 h), 240 °C (1 h), 260 °C (1 h), 280 ° C (2 h), 300 °C (1 h) under an atmosphere of nitrogen. After that, dark

View Article Online
DOI: 10.1039/C4RA12694G

brown thermosets were obtained. The thermosets was placed in a ceramic holder and was then pyrolyzed at 1500 °C for 2 h in a flowing of nitrogen with a heating rate of 10 °C/min.

Simulation details

ReaxFF parameters for carbon, hydrogen, oxygen and boron were taken from a previously optimized data set. A total of 8 PB polymeric chains with 3 repeating units were placed in a periodic box of 25.14Å×25.14Å×25.14 Å, giving a density of 0.88 g/cm^3, which was consistent with the experiment results. In addition, B-Cl bonds are replaced by B-OH which has the advantage that only C, H, O, B are involved, so that the ReaxFF force field is better calibrated and validated. Then, the system was energy-minimized to a force tolerance of 1 kcal/mol/Å by using smart minimization. The system was equilibrated at 300 K with an NVT simulation for 40 ps. In this way, each system was brought to an equilibrium density that matches the experimental value. After that, NVT simulation was also performed from 0 to 4300 K at a heating rate of 100 K/ps with a time step of 0.2 fs to obtain the structure evolution of PB thermosets. To obtain the carbonized microstructure of PB thermosets, the above energy-minimized system was equilibrated at 3300 K with an NVT simulation for 40 ps. The temperature was kept constant by using a Berendsen thermostat with coupling constant of 100 fs.

Molecular Modelling Software

The Materials Studio molecular modelling suite (Accelrys Inc.) was utilized in this work using in house PCs (Inter Xeon E3-1230 3.30GHz，8GB RAM, 500 GB HDD).

Characterization

Fourier transform infrared spectrum (FT-IR) was recorded in a range of 4000-400 cm^{-1} with a Bruker Equinox 55 FTIR by potassium bromide (pellets). The ^{1}H, ^{13}C and ^{11}B NMR analyses were run on a Bruker Avance 300 (300 MHz for 1H and 75.5 MHz for ^{13}C) and Bruker Avance 400 (115.6 MHz for ^{11}B) in DMSO solution. Differential scanning calorimetry (DSC) experiments were carried out on Q1000 from TA Instruments at a heating rate of 10 °C/min from room temperature to 350 °C with a N_2 flowing rate 60 mL/min. The DSC was used to study the nonisothermal curing at 5, 7.5, 15 and 20 °C/min up to 350 °C. The degree of cure of PB precursor, α, and the reaction rate, $d\alpha/dt$, were calculated as follows.

$$\alpha = \frac{\Delta h_T}{\Delta h_{total}} \qquad (1)$$

$$\frac{d\alpha}{dt} = \frac{dh/dt}{\Delta h_{total}} \qquad (2)$$

where Δh_T and Δh_{total} are the heat evolved during a dynamic curing up to a temperature T and the total heat released during curing respectively, and dh/dt is the instantaneous heat flow released at a temperature T.

The residual heat Δh_{res}, which allowed to determining the degree of conversion as:

$$\alpha = 1 - \frac{\Delta h_{res}}{\Delta h_{total}} \qquad (3)$$

Glass transition temperature (T_g) was determined from the second heating run with the point of inflection method. To remove water vapor and thermal history, PB precursor was heated from room temperature to 80 °C, then it was cooled to room temperature, followed by a second heating from room temperature to 180 °C. T_g of PB thermosets was determined with the similar method as that of PB precursor. PB thermosets was heated from room temperature to 300 °C to eliminate the heat history, then it was cooled to room temperature, followed by a second heating from room temperature to 350 °C with a heating rate of 10 °C/min. Thermogravimetric analysis (TGA) was performed on a TA Instrument of STA 409PC at a heating rate of 10 °C/min from room temperature to 800 °C under an atmosphere of nitrogen and air. TGA coupled with FT-IR spectroscopy (TGA-FTIR) was carried out on TGA/STA449-F3 from NETZSCH interfaced with a Vertex 70 FT-IR spectrometer at a heating rate of 10 °C/min. X-ray powder diffraction (XRD) measurements were conducted with a Bruker D8 equipment. The average size of the crystallites was calculated from the Scherrer equation

$$L_{hlk} = \frac{K\lambda}{(\beta \cos\theta)} \qquad (4)$$

where K is taken as 0.9 for (00) peak and 1.84 for (10) peak, λ is the wavelength ($\lambda = 0.154$ nm), θ is the bragg angle and β is the width at mid-height. X-ray photoelectron spectroscopy (XPS) experiments were carried out at an Axis Ultra DLD system. The elemental composition was determined from the curve-fitting C 1s, B 1s and O 1s multiplex spectra, respectively.

Results and discussion

Synthesis and characterization of PB precursor

PB was prepared following the route as depicted in Scheme 1. PB precursor was prepared by a polycondensation reaction between dipropargyl ether bisphenol A and BCl_3. As is known, the degree of polymerization in this case is largely controlled by the stoichiometric mole ratio. Depending on the stoichiometric ratio, PB precursor can be either viscous gel or solid powder. Solid PB powders can be obtained when the stoichiometric molar ratio of BCl_3 to dipropargyl ether bisphenol A di-lithium is 1, while the precursor is viscous gel as the ratio is 1.7. The composition of PB precursor has significant influence on the thermal properties of the resulting PB thermosets. To guarantee excellent thermal stability of the resulting PB thermosets, solid PB was chosen as a model precursor polymer for the rest of the research. PB precursor is readily soluble in such organic solvents as acetone, THF, DMF, DMSO. The structure of PB precursor is confirmed by FT-IR, ^{1}H NMR, ^{13}C NMR and ^{11}B NMR. FT-IR spectrum of PB precursor reveals the C-B, B-Cl, Ar-O and C-O characteristic absorptions at 1154, 744, 1253 and 1028 cm^{-1}, respectively (Fig. 1(a)). In addition, the absorptions which are attributed to O-H and C=C groups appear at 3421 and 1693 cm^{-1}, respectively. The weak absorption at 1396 cm^{-1} indicates the existence of H_2O or B-OH units that might come from the moisture absorption or the hydrolysis of the B-Cl groups of PB.

ARTICLE View Article Online DOI: 10.1039/C4RA12694G Journal Name

Additionally, alkenyl and B-Cl moieties are likely to undergo inter-polymer reactions via chloroboration and cyclization ($2\pi+4\pi$ electrons) [14]. The absorption of C=C at 2966 cm^{-1} might relate to the inter-polymer reactions of alkenyl and B-Cl moieties presented in PB.

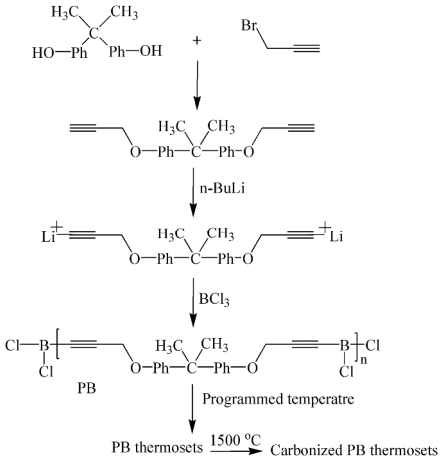

Scheme 1. Schematic representation of synthesis of PB, PB thermosets and the subsequent carbonization of PB thermosets.

To further confirm the existence of H_2O and elucidate the origin of B-OH and C=C, ^{1}H, ^{13}C and ^{11}B NMR analyses were performed. ^{1}H NMR chart of PB is showed in Fig. 1(b) where the signal ranged from 6.90 to 7.12 ppm is assigned to aromatic protons. The peak at 4.75 ppm is attributed to the protons of methylene of propargyl group. The characteristic peak resonance at chemical shift of 1.50 ppm is corresponded to the protons of $-CH_3$ originated from bisphenol A. The peaks at 9.5 and 3.62 ppm were ascribed to the protons of B-OH and H_2O, respectively, which were consistent with the FT-IR analysis. In addition, ^{13}C NMR chart of PB (Fig. 1(c)) shows the corresponding resonances at 75.36 and 78.77 ppm, indicating the presence of propargyl structure. It should be noted that the weak peaks that assigned to carbon atoms of C=C groups as referred in FT-IR spectrum, were also detected at 127 ppm (m) and 115 ppm (m'), supporting the presence of cyclic oligomer in addition to the majority of PB precursor. Boron atoms of PB precursor are further confirmed as show in Fig. 1(d) with the resonance at 18 ppm. The narrow line at 1.5 ppm is attributed to a boron site of tetrahedral symmetry that might be associated with an ion complex between B species and LiCl [23], while a broad background resonance can be found broad peak at 0 ppm.

Both FT-IR analysis and NMR results confirm that PB has been successfully synthesized with the schematic structure as showed in Scheme 1. PB contains propargyl groups in the main chain, to allow for achieving boron-containing ablative material via pyrolysis and carbonization of the PB thermosets. To obtain a better insight into the cross-linking and the chemical structure of the carbonized PB thermosets, thermal property of the thermosets is investigated in the first place.

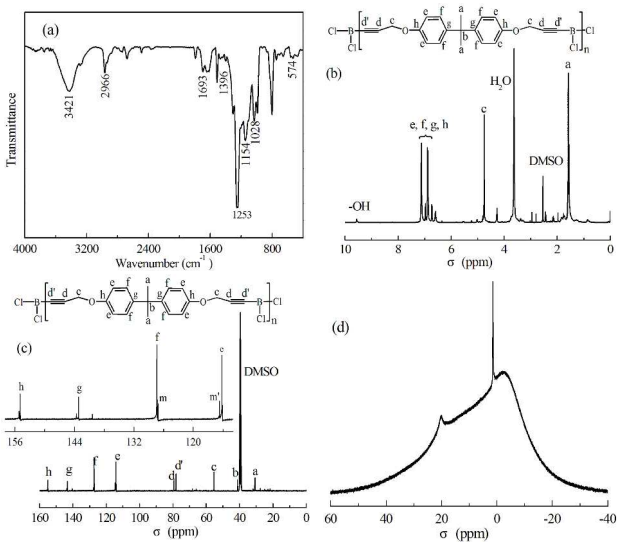

Figure 1 Fourier transform infrared (FT-IR) spectrum of PB precursor (a). Nuclear magnetic resonance (NMR) chart of PB precursor showing the characteristic protons: ^{1}H NMR (b), ^{13}C NMR (c), and ^{11}B NMR (d).

Thermal Properties of PB precursor and PB Thermosets

DSC was used to investigate the cure behavior of PB precursor at different heating rate of 5, 7.5, 15, and 20 °C/min for practical purposes. Figure 2(a) demonstrates the DSC curves of PB precursor at the four different heating rates. PB precursor exhibited an exotherm with onset at 220-238 °C and peak at 268.5-292 °C, corresponding to the cross-linking of propargyl unit of PB at each of the heating rate. Increase heating rate causes the exothermic peak to shift to a higher temperature because of thermal hysteresis. All reaction enthalpies can be obtained by integration of each of the peak area of different heating rates. The reaction enthalpies are hardly affected by the heating rate, and they changed within a range of 326.3-376.5 J/g. These results illustrates that although the curing rates are sensitive to the reaction temperature, the nonisothermal cure can achieve nearly to the same ultimate reaction extent. The conversional curves as a function of heating time for non-isothermal reaction of PB precursor at the different heating rates are obtained from Eq. (1) and (2), as indicated in Fig. 2(b). The conversion degrees increase relatively slower at the beginning of the reaction, after which the increase in conversion become much faster; eventually, the conversion curve levels to horizontal line with a constant conversion degree of unity. Increasing the heating rate causes the conversional curve shifting to the decreased time zone and become steeper, which suggests that the curing reaction rate increases with the heating rate.

Prediction of the isothermal cure of PB precursor is of great application importance in industrial area. Such information can be applied in processing condition optimization while ensuring the complete curing of products. DSC traces after each polymerization cycle was also evaluated as displayed in Fig. 2(c). PB precursor exhibited an exotherm with onset at 221.3 °C

View Article Online
DOI: 10.1039/C4RA12694G

and peak at 279.5 °C under the heating rate of 10 °C/min. This exotherm corresponds to the cross-linking of propargyl unit of PB, and the peak cure temperatures are slightly higher than that of the conventional phenolic monomers, suggesting the low reactivity due to the lower mobility of the PB precursor. It is evident that the exothermic peak gradually decreases after each polymerization cycle and disappears by the end of the heating at 300 °C/1 h (Fig. 2(d)). The absorption band of the C≡C group in the PB polymer emerges at 2120 cm^{-1}. The disappearing of the band after heating cycle of 300 °C/1 h is also the evidence that the cure was finished. Therefore, both DSC and FTIR results indicate that the polymerization of PB precursor is effectively completed by the end of the heating cycle.

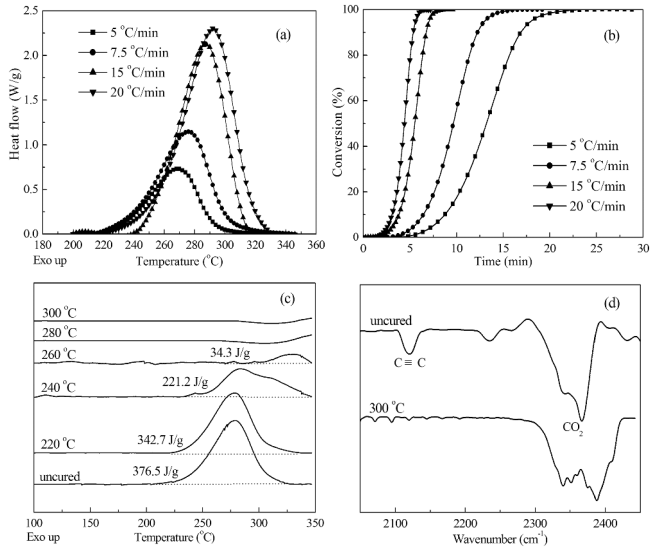

Figure 2 Differential scanning calorimetry (DSC) plot (a) and evolution of conversion against time (b) of PB precursor at different heating rates. DSC plots of PB precursor after curing at different temperature (c). Disappearance of absorption band of C≡C on PB after the cure cycle of 300 °C to verify the finish of cure reaction(d).

The T_g values of PB precursor and PB thermosets were determined from DSC curves (Fig. 3(a)). PB precursor showed a T_g value of 128 °C, while the value of PB thermosets is 294 °C. The high T_g of PB thermosets is due to the cross-linking of PB precursor which restricted mobility of PB chains after curing. Thermal as well as thermo-oxidative stability of PB precursor and PB thermosets were evaluated by TGA analysis under both N_2 and air environment. Figure 3(b) illustrated the weight loss and the derivatives of the weight loss curves. It is revealed that all the polymers lost trapped solvent and residue water at around 60-100 °C (as evidenced by the FTIR data) in both atmospheres, but the weight loss underwent different degradation mechanisms at high temperatures. PB precursor exhibits 10% weight loss at temperature (T_{d10}) of 356 °C in air and 359 °C in N_2, respectively, while the weight loss for PB thermosets is at 416 and 465 °C, respectively. After cure, the thermal stability of PB precursor was improved greatly. For instance, PB thermosets has outstanding thermal stability with T_{d5} of 416 °C under N_2, and the weight residue of PB thermosets at 800 °C under N_2 is 74.0%, which is higher than that of PB precursor (54.2%). In addition, in all cases, the weight loss in air is larger than in N_2 for both PB precursor and PB thermosets. The observed variations in the thermal stability with the present of oxygen can be correlated to the complex thermo-oxidative reactions along with the producing of CO, CO_2 and H_2O. But differences were observed as for PB precursor polymer and PB thermosets. For instance, as for PB precursor, thermal oxidative degradation occurred after the degradation of the aromatic carbon in air and left as low as 22.8%, while the decomposition of PB thermosets gave a char yield of 56.7% in air, indicating very good thermo-oxidative stability as expected for boron-containing thermosets. In the case of PB thermosets, branching and crosslinking in addition to the presence of boron atoms appeared to slow down the degradation in oxidative environment. The degradation steps of PB precursor and PB thermosets in air and in N_2 are also presented in Fig. 3(b) from the derivatives of the weight loss. The initial main degradation temperature of PB thermosets is 83 °C higher than that of PB precursor in air. While in N_2, the initial main degradation temperature of PB thermosets is 140 °C higher than that of PB precursor. A bimodal peak dominates the degradation process at high temperature of 400-600 °C, which was estimated to be initiated at the ether linkage and the scission of methylene of bisphenol A with further heating. The excellent thermal stability of PB thermosets is originated in part from the high thermal stability of main chain propargyl moieties. Meanwhile, the presence boron atoms can be an explanation for the observed enhancement in the thermo-oxidative stability of PB thermosets. It should be noted that the weight losses of PB thermosets in the temperature range of 600-800 °C are only 6.0% in N_2 and 7.8% in air atmosphere, respectively. Meanwhile, PB thermosets has a weight residual of 74% in N_2 at 800°C, which is close to that of PAA (80%) [24] and higher than that of boron containing phenolic resin (70%). The outstanding thermo-oxidative stability of PB thermosets suggests that PB can be an excellent precursor resin for carbon based composites.

To illustrate the evolution and the chemical nature of PB thermosets during pyrolysis, TG-FTIR technology was performed at different temperatures under inert atmosphere. As shown in Fig. 3(c), H_2O (3964-3500 cm^{-1} and 1854-1500 cm^{-1}) and CO_2 (2360-2320 cm^{-1}) existed during the whole pyrolysis. Before 300 °C, H_2O was the predominant volatile originated from the absorbed water of PB thermosets. As the pyrolysis proceeded stepwise beyond 300 °C, H_2O was produced by complicated reactions. Two new bands at 3000-2600 cm^{-1} and 1325-500 cm^{-1} which are assigned to CH_4 appear when the decomposition advances to 400 °C [25]. The characteristic absorption at 1845-1500 cm^{-1} indicates the existence of gases attributed to alkene, which implies that benzene ring started to decomposition. In addition, the spectra exhibits the vibrancy of C=O at 1850-1600 cm^{-1} due to the formation of such carbonyl compounds as aldehyde, ketone and carboxylic acide as the decomposition reaching maximum at 400-600 °C. When the sample was heated to 600 °C, the peaks of CH_4 and alkene become weak. The new peak at 2250-2000 cm^{-1} is assigned to

View Article Online
DOI: 10.1039/C4RA12954G
Journal Name

CO, indicating the generation of aromatization of PB thermosets. By means of TG-FTIR analysis the significant evolution of PB thermosets under N_2 atmosphere has been identified and the pyrolysis of the thermosets can be divided into two stages. The first one is in the temperature range of 400-600 °C. The decomposition was started by losing such carbonyl compounds as aldehyde, ketone and carboxylic acide due to the cleavage of ether bond and aliphatic chains. In addition, benzene ring in PB began to decomposition, leading to the formation of alkene. The other one is in the temperature range of 600-800 °C, with the formation of a high degree network and the simultaneous generation of carbonic oxide.

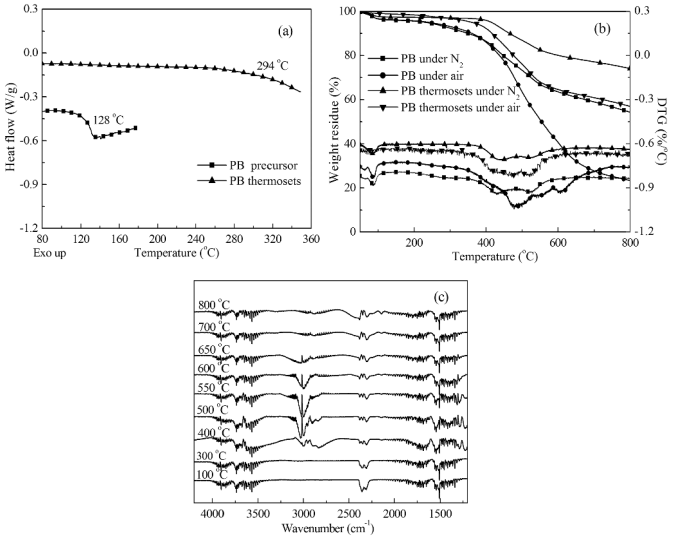

Figure 3 Differential scanning calorimetry (DSC) plot for determining T_g of PB precursor and PB thermosets (a). Thermal gravity analysis (TGA) and the derivative weight loss of PB precursor and PB thermosets under a flowing of nitrogen and air (b). TG-FTIR spectra of PB thermosets (c).

ReaxFF molecular dynamics simulation has been quite successfully applied to solve a variety of chemical problems, including thermal degradation of polymers. To further understanding the pyrolysis of PB thermosets on molecular level, ReaxFF-MD simulation was performed, and the simulation detail was show in section of Simulation Details. The main steps of thermal decomposition of PB thermosets observed in ReaxFF-MD are displayed in Fig. 4. The aliphatic ether bond first broke at 12 ps, which was consistent with the TG-FTIR results. Few aromatic ether bonds broke at the end of 20 ps due to the instability of aromatic ring containing five electrons. As the temperature increased, at about 28 ps (2800 K), methyl began to cleave from bisphenol A structure, leading to amount of $CH_3^{\cdot}$. As a result, methane was produced due to the combination of $CH_3\cdot$ with hydrogen. When the temperature further heightened, at about 31 ps (3100 K), benzene ring in PB thermosets started to cleave, which resulted in the formation of alkene and carbonyl compounds. Results from ReaxFF-MD simulation follow the trends of TG-FTIR analysis and provide insights on the involved reaction pathways of PB thermosets.

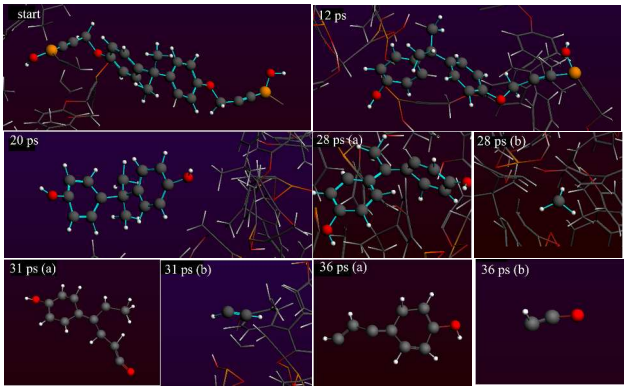

Figure 4 Snapshot of the ReaxFF simulated pyrolysis and the evolution of major reaction products of PB thermosets at different time (Color code: C, grey; O, red; H, white, B, yellow).

Microstructure analysis of carbonized PB thermosets

PB thermosets exhibits a high char yield under pyrolytic conditions. Further development of PB thermosets requires fundamental understanding of the molecular processes, and the subsequent char evolution under pyrolytic conditions. In order to study the nature of chemical environment of the carbonized PB thermosets near to the surface, XPS measurement was adopted. The XPS spectra were deconvoluted using a Gaussian distribution. The C 1s spectrum (Fig. 5(a)) presented four peaks centered at 283.5, 284.4, 285.1, 286.2 and 288.6 eV, respectively. The binding energy of 283.5 and 284.4 eV corresponded to the C-B and C-C bonds in graphite [26], whereas the binding energy of 285.1 eV was assigned to C-C bonds of disordered carbon [27]. The peak at 286.2 eV was characteristic of the C=O and the peak near 288.6 eV were mainly from O-C=O. Using the intensities for each element from the spectra and correcting them by the sensitivity factors, a quantitative composition can be proposed. It should be noted that the proportion of graphite carbon was 65.14%, which was higher that of disordered carbon. The B 1s XPS spectrum (Fig. 5(b)) of the sample also exhibits broad bands covering the region of C-B. In addition, the asymmetrical B 1s peaks centered at 192.3, 190.5 and 189.6 eV (B-C) indicate that the boron atoms in the sample were in different chemical environments. The higher binding energy of the component at 192.3 eV is attributed to the presence B_2O_3. It is revealed that the peak at 190.5 eV most likely corresponds to boron species with mixed B-C and B-O bond [28]. O 1s feature at 533.0 eV relates to a B-O bond that could be from the progressive oxidation of the surrounding pyrolytic boron (Fig. 5(c)). A corresponding O1s component associated with the C-O bond appeared at 531.8 eV. These XPS results confirmed that the carbonized PB thermosets is composed with different C-C, B-C and B-O chemical bonds to form the graphite-like B-C-O atomic hybrid configurations. X-ray diffraction patter can provide information about the crystallite parameters of interlayer spacing of (002) peak (d_{002}) and crystallite size (L_c) of carbon materials. As shown in Fig. 5(d), after the PB thermosets was carbonized at 1500 °C for 2 h, two peaks at 2θ

View Article Online
DOI: 10.1039/C4RA12694G

angles of about 26.10 ° and 42.52 ° appeared, corresponding to the diffraction of (002) and (100), respectively, which are consistent with the standard X-ray powder diffraction pattern of carbon. The carbonized PB thermosets exhibits a small crystalline size with a L_c of 3.15 nm after pyrolysis at 1500 °C, which might be associated with the existence of LiCl. This speculation can be verified by the intense peak appeared at 34.12 °, corresponded to the crystalline state of LiCl by referring to the card of PDF2-2004. LiCl is difficult to remove during the pyrolysis, and the presence of LiCl impurity may inhibit the graphitic crystallinity [23]. The d-spacing of carbonized PB thermosets is about 0.3416 nm, which is between the size of disordered carbon (0.3440 nm) and graphitic carbon (0.3354 nm). The carbonized PB thermosets was partly graphitizing, which indicated that boron atom might promote the graphitization of PB thermosets. The carbonization process of PB thermosets involves a complex sequence of reactions, and further computational modelling of the resin-to-char process can provide insights into the involved reaction barriers and pathways.

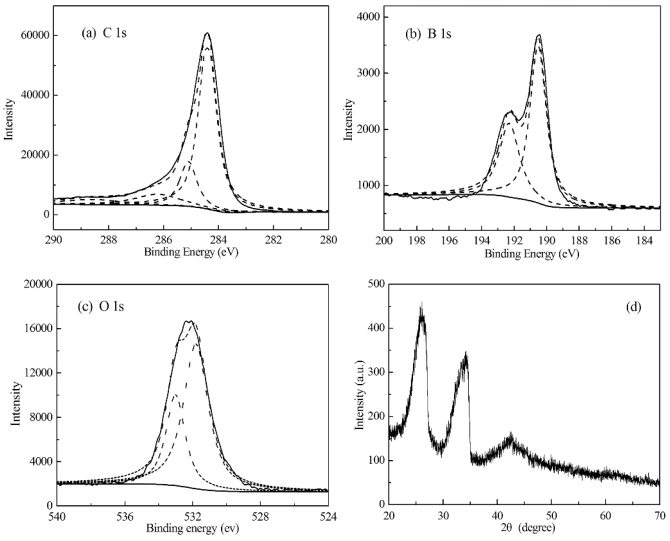

Figure 5 C 1s (a), B 1s (b), and O 1s (c) X-ray photoelectron spectroscopy (XPS) of the carbonized PB thermosets (solid line) together with the single Gaussian curve and the deconvoluted component curves (broken line) at 1500 °C for 2 h in a flowing of nitrogen. X-ray diffraction (XRD) of PB thermosets after carbonized at 1500 °C for 2 h in a flowing of nitrogen (d).

In order to better understand the microstructure and the reaction mechanism on the atomic level, the carbonization process of PB thermosets was studied using ReaxFF-MD simulation. Firstly, the temperature zone that influences the stability of the graphitic precursor was identified and the chain disintegration was investigated. At the start of the simulation run, the equilibrated structures have 8 chains with a carbon chain length of 63. High temperature simulations at 3 different temperatures in the range of 2700-3500 K were performed. Figure 6(a-c) shows the number of fragments as a function of carbon chain length simulated at temperature of 2700, 3100 and 3500 K for 20 ps. After 20 ps simulation at the temperatures, polymerization occurs between polymer chains resulting in longer chains of carbon chain length from 48 at 2700 K up to 107 at 3100 K, and the carbon length decreases to 14 at 3500 K. However, C_2 molecules production is enhanced with time at the three temperatures. This result indicates that all the long chains break into smaller, shorter chains in that the temperature is too high to promote the formation of graphitic network. To estimate the temperature range for a higher probability of graphitization, the total number of C_2 molecules formed after 20 ps is plotted as a function of temperature and the data points is extrapolated to intersect the x-axis (temperature axis). The intersection occurs at 2620 K is a sign that below the temperature, stable graphitic structure can be formed via avoiding breaking of polymers into smaller molecules (Fig. 8(d)).

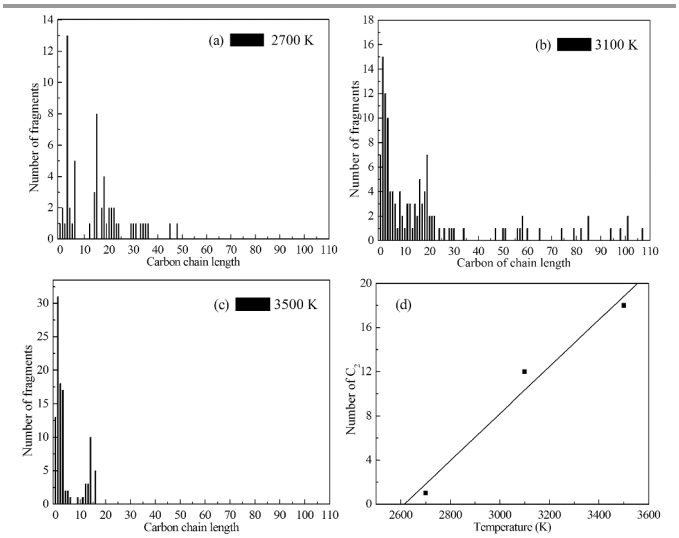

Figure 6 Number of fragments as a function of carbon chain length simulated at different temperature (a-c). The number of C_2 molecules formed after 40 ps is potted as a function of temperature (d). On extrapolating the slope, it intersects on the x-axis at 2620K, suggesting the existence of two temperature zones, disintegration (temperature lower than 2620 K) and polymerization (with temperature higher than 2620 K).

To avoid the pyrolysis reaction, NVT-MD simulation was performed at 2300 K via using a partially pyrolyzed structure an initial structure, which was run at 2700 K for 20 ps after equipping at 300 K for 20 ps (Fig. 7(a)). In the study, the NVT ensemble were performed in a closed simulated system, while experiment analyses are usually conducted under a continuous inert gas flow, which takes away pyrolysis products. So, the small molecules such as CO_2 and H_2O were removed manually during the simulation. Although our simulation did not show many pyrolysis reactions happening at 2300 K, large patches of graphitic or fullerene-related structures are not observed. The main reason leading to the result is that our simulation time frame is relatively short (20 ps) which is a limit of the time-scale problem in all molecular dynamics methods. Despite the time-scale limitation, a graphitic fragment containing 6 fused rings with 5 to 7-membered rings was captured after 2.72 ns run of MD simulation, as shown in Fig. 7(b). This small patch can act as a seed for the formation of large graphitic fragments with the increase of the simulation time.

View Article Online
DOI: 10.1039/C4RA12954G
Journal Name

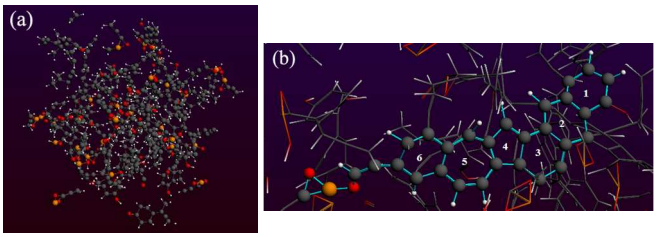

Figure 7 Snapshot of the initial structure obtained from a pyrolyzed structure of PB thermosets simulated for 20 ps at 2700 K (a). Snapshot of a graphitic fragment containing 6 fused rings after the initial structure simulated for 2.72 ns at 2300 K (b) (Color code: C-grey, O-red, H-white, B-yellow).

To identify the effect of boron atom on the carbonization and the detail changes of boron connections during the process, chemical bonding of boron atoms are captured as shown in Fig. 10. Firstly, it can be seen that boron atom exists with a O-B-C three-membered ring (Fig. 8(1)). As the simulation time increases, one B-O bond forms on the three-membered ring (Fig. 8(2)). Subsequently, C-O bond forms due to its low bond energy (Fig. 8(3)). Meanwhile, another B-O bond generates (Fig. 8(4)), leading to the final structure as displayed in Fig. 8(5). Combined the simulation results with XPR analysis, it can be concluded that boron atoms substitute into the graphitic structure with such three forms as B_2O_3,  or  .

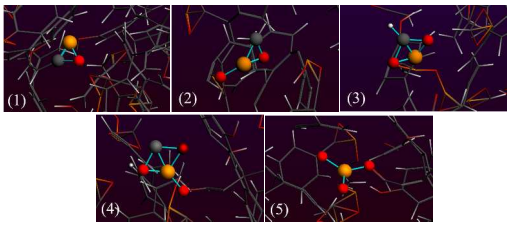

Figure 8 Changes of chemical bonding of boron atom as a function of simulation time (Color code: C, grey; O, red; H, white; B, yellow).

To sum up, ReaxFF-MD simulation combined with experimental analysis are effective for understanding the evolution of graphitic precursor and the resulting carbonized structure (Fig. 9). This strategy via using MD simulation as well as experimental analysis is particularly valuable for understanding such factors contributing to thermal stability as either through enhancing graphitization or by blocking active site with protective boron oxide layer at the surface.

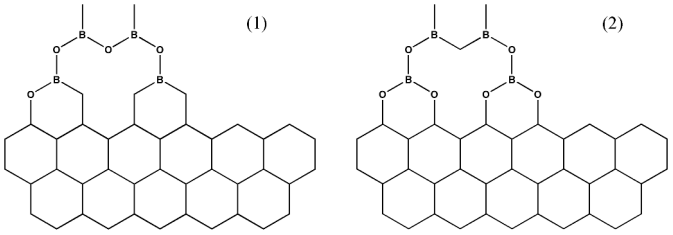

Figure 9 Schematic representations of the carbonized structure of PB thermosets.

Conclusions

In this study, a novel dipropargyl ether bisphenol A boron-containing polymer (PB) was synthesized and characterized using FTIR and NMR analyses. Thermal cure of PB was achieved via the propargyl groups. The as-synthesized PB thermosets exhibits outstanding thermal stability, with a $T_{d5\%}$ of 416 °C and a weight residue of 74.0% at 800 °C under N_2. TG-FTIR and ReaxFF-MD were performed to discuss the pyrolysis and evolution as well as the chemical nature of the PB thermosets. During pyrolysis, PB thermosets can transform into polyaromatic domains companying with the release of such gases as water, CO_2, CO, and CH_4. Formation of large stable graphite containing 6 fused rings was captured at 2300 K during a simulation run of 2.72 ns. The carbonized structure is partly graphitizing, and boron atoms inserted into graphitic fragment with the bonding of B_2O_3 and C-B-O. The study demonstrated that ReaxFF-MD simulation can provide useful insights into the structure of carbonized materials and presents the way how boron atoms incorporate into the fused rings.

Acknowledgements

The authors acknowledge the National Science Foundation of China (No. 51103114) for financial support.

Notes and references

[a] Department of Chemical Engineering, School of Chemical Engineering and Technology, Xi'an Jiaotong University, Xi'an 710049, China
Corresponding author: liuyuh@mail.xjtu.edu.cn (Y. H. Liu)

1 Mishnaevsky, J. L.; Dai, G. *Comp. Mater .Sci.* 2014, **81**, 630.
2 Hao, W,; Huang, J. F.; Cao, L. Y.; Yin, L. X.; Wu, J. P.; Fei, J. *Ceram. Int.* 2013, **39**, 9797.
3 Yu, H. Y.; Lu, J. H; Song, Q.; Li, K. Z.; Li, H. J.; Fu, Q. G.; Zhang, L. L. *Vacuum* 2014, **99**, 76.
4 Katzman, H. A.; Mallon, J. J.; Barry, W. T. *J Adv Mater* 1995, **2**, 21.
5 Westwood, A; Rand, B.; Lu, S. *Carbon* 2004, **42**, 3071
6 Jacobson, N. S.; Roth, D. J.; Rauser, R. W.; Cawley, J. D.; Curry, D. M. *Surf. Coat Technol.* 2008, **203**, 372.
7 Smeacetto, F.; Ferraris, M.; Salvo, M. *Carbon* 2003, **41**, 2105.
8 Chu, Y.; Li, H.; Fu, Q; Wang, H.; Hou, X.; Zou, X.; Shang, G. N. *Carbon* 2012, **50**, 1280.
9 Li, K. Z.; Lan, F. T.; Li, H. J.; Shen, X. T.; He, Y.G. *J. Eur. Ceram. Soc.* 2009, **29**, 1803
10 Zhong, D. H., Sano, H.; Uchiyama, Y.; Kobayashi, K. *Carbon* 2000, **38**, 1199.
11 Lee, Y.; Radovic, L. R. *Carbon* 2003, **41**, 1987.
12 Ye, L.; Han, W.; Zhang, R.; Hu, J.; Zhao, T. *J. Appl. Polym. Sci.* 2008, **110**, 4064.
13 Cermignani, W; Paulson, T. E.; Onneby, C.; Pantano, C. G. *Carbon* 1995, **33** 367
14 Wang, J.; Guo, Q.; Liu, L.; Song, *J. Int. J. Adhes.* 2005, **25**, 495.
15 Chasmawala, M.; Chung, T. C. *Carbon* 1997, **35**, 641.
16 Desai, T. G; Lawson, J. W.; Keblinski, P. *Polymer* 2011, **52**, 577
17 Mijovic, J.; Zhang , H. *J. Phys. Chem. B* 2004, **108**, 2557

Journal Name View Article Online DOI: 10.1039/C4RA12694G ARTICLE

18 Fan, H. B.; Yuen, M. M. F. *Polymer* 2007, **48**, 2174
19 Tack, J. L.; Ford, D. M. *J. Mol. Graphics Modell* 2008, **26**, 1269
20 Ho, S. R.; Aoyagi, M. *Macromol. Theory. Simul.* 2013, **22**, 443.
21 Qi, T. T.; Bauschlicher, C. W.; Lawson, J. J. W.; Desai, T. G.; Reed, E. J. *J. Phys. Chem. A* 2013, **117**, 11115.
22 Jiang, D. E.; Duin, A van; Goddard, W. A.; Dai, S. *J. Phys. Chem. A* 2009, **113**, 6891
23 Chung, T. C. M.; Jeong, Y.; Chen, Q.; Kleinhammes, A.; Wu, Y. *J. Am. Chem. Soc.* 2008, **130**, 6668.
24 Yan, L. S.; Zhang, X. H; Li, H.; Cui, H. *J. Adv. Mater-Covina* 2007, **3**, 22
25 Salema, A. A.; Afzal, M. T.; Motasemi, F. *J. Anal. Appl. Pyrol.* 2014, **105**, 217-26.
26 Hu, R.; Chung, T. C. M. *Carbon* 1996, **34**, 1181.
27 Ottaviani, B; Derre, A; Grivei, E.; Mahmoud, O.; Guimon, M. F.; Flandrois, S.; Delhaès, P. *J. Mater. Chem.* 1998, **8**, 197
28 Cermignani, W.; Paulson, T. E.; Onneby, C.; Pantano, C. G. *Carbon* 1995, **33**, 367